Direct measurement of the Wigner function by photon-number-resolving detection

Niranjan Sridhar,[1,*] Reihaneh Shahrokhshahi,[1] Aaron J. Miller,[2] Brice Calkins,[3] Thomas Gerrits,[3] Adriana Lita,[3] Sae Woo Nam,[3] and Olivier Pfister[1]

[1]*University of Virginia, Department of Physics, 382 McCormick Rd., Charlottesville, Virginia 22903, USA*
[2]*Albion College, 611 E. Porter St., Albion, Michigan 49224, USA*
[3]*National Institute of Standards and Technology, 325 Broadway, Boulder, Colorado 80303, USA*
**Corresponding author: ns4mf@virginia.edu*

Received July 11, 2014; revised September 2, 2014; accepted September 3, 2014;
posted September 12, 2014 (Doc. ID 216428); published September 25, 2014

Photon-number-resolving (PNR) detection allows for the direct measurement of the Wigner quasi-probability distribution of an optical mode without the need for numerically processing an inverse Radon transform [Phys. Rev. Lett. **76**, 4344 (1996)]. In this work, we reproduced the seminal experiment of Banaszek *et al.* [Phys. Rev. A **60**, 674 (1999)] of quantum tomography of a pure coherent state, and of a statistical mixture thereof, and extended it to the more general case of photon fluxes with much more than one photon per detection time. This was made possible by the use of a superconducting transition-edge sensor to perform PNR detection from zero to five photons at 1064 nm, at ~70% system efficiency and with no dead time. We detail signal acquisition and detection efficiency and discuss prospects for applying such quantum tomography to non-Gaussian states.

OCIS codes: (270.5570) Quantum detectors; (270.0270) Quantum optics; (270.5290) Photon statistics.
http://dx.doi.org/10.1364/JOSAB.31.000B34

1. INTRODUCTION

The complete characterization of the quantum state, a.k.a., quantum state tomography or quantum tomography, of a physical system plays a key role in physics, in particular in quantum information. Early on, optical systems naturally lent themselves to quantum tomography, likely due to the classical prevalence of their wave nature. The particular case of continuous variables constituted by the canonically conjugate amplitudes of the quantized electromagnetic field is well known. In this case, access is gained to the amplitude and phase quadrature field operators, $Q = (a + a^\dagger)/\sqrt{2}$ and $P = i(a^\dagger - a)/\sqrt{2}$, by way of homodyne detection of this quantum field with a local oscillator (LO)—in practice a well-stabilized laser field. The measurement histograms of a sufficient number of rotated field quadratures represent marginal probability distributions of the Wigner quasi-probability distribution [1], which can then be reconstructed using numerical inverse Radon transform post-processing [2–4].

An alternate and more direct method to measure the Wigner function free of the encumbrance of the reconstruction process [5] was proposed by Banaszek and Wódkiewicz [6], and also by Wallentowitz and Vogel [7]. This method relies on ideal photon counting, a.k.a., photon-number-resolving (PNR) detection, defined as an ideal measurement in the Fock state basis.

This requires the experimental capability of photon number resolution, which also implies, in principle, unity quantum detection efficiency since Fock states form an orthogonal basis. It is important to note, however, that the effect of losses (and thus of nonideal detection efficiency) can be, in principle, deconvoluted exactly in the general case if the overall efficiency is larger than 50% [8], and at the cost of taking additional data. In the particular case of states whose nature is invariant under losses (e.g., nonsqueezed Gaussian states such as coherent states), Bondani *et al.* showed that linear photodetectors with intrinsic gain can be used to perform analysis of classical states [9,10].

The arduous experimental requirement of achieving PNR was circumvented by use of detectors with single-photon sensitivity, such as photomultipliers or avalanche photodiodes, both in the Geiger mode. Since such detectors do not, in most cases, resolve the photon number, one also has to work at photon fluxes low enough that there would be a negligible probability of more than one photon in the detection's temporal window. Under such conditions, Banaszek *et al.* demonstrated coherent-state quantum tomography [11] with an effective restriction to the $\{|0\rangle, |1\rangle\}$ subset of the Fock basis. More recently, the quantum properties of pulsed light fields were also investigated point by point in phase space [12]. When the input has higher photon flux, one can also reach PNR by splitting a multiphoton input [13] onto efficient single-photon detectors whose count is integrated [14,15].

Our ultimate goal is to achieve unconditional direct-detection state tomography using highly efficient PNR detectors. As a preliminary demonstration, we reproduced Banaszek's seminal experiment on coherent states with a superconducting transition edge sensor (TES) of system detection efficiency above 90% [16]. These detectors can distinguish between zero- to five-photon Fock states at 1064 nm with high system detection efficiency, no dead time, and near zero dark count. Recently, the TES was quantum characterized to be a linear detector [17]. Therefore, the TES can measure the state without any fair sampling assumption. We believe this to be a step toward more direct state reconstruction of nonclassical

states (i.e., with minimal numerical postprocessing) which, to the best of our knowledge, has not yet been achieved.

In the next section, we outline the theoretical foundation of quantum tomography with PNR measurements. In Section 3, we describe the TES detector and the acquisition and processing of PNR signals. In Section 4, we describe the quantum tomography experimental setup and present the measurement results. In Section 5, we discuss experimental limitations (losses) and we conclude.

2. QUANTUM TOMOGRAPHY BY COUNTING PHOTONS [6]

The Wigner function [1] of a single mode of the quantum electromagnetic field of density operator ρ can be written [3] as

$$W(q,p)=\frac{1}{2\pi}\int_{-\infty}^{\infty}e^{iyp}\left\langle q-\frac{y}{2}\middle|\rho\middle|q+\frac{y}{2}\right\rangle \mathrm{d}y, \tag{1}$$

where $|q\pm y/2\rangle$ belongs to the amplitude quadrature eigenbasis. If we write $\rho=\sum_{n,n'}\rho_{nn'}|n\rangle\langle n'|$ in the Fock basis and use the Hermite polynomial expression of the (here, amplitude) quadrature-Fock Clebsch–Gordan coefficients [18],

$$\langle q|n\rangle=\pi^{-\frac{1}{4}}(2^n n!)^{-\frac{1}{2}}e^{-\frac{q^2}{2}}H_n(q), \tag{2}$$

where $H_{n(q)}$ is the Hermite polynomial of order n. It is then straightforward to obtain the following remarkable relation from the orthogonality of Hermite polynomials:

$$W(0,0)=\frac{1}{\pi}\sum_n(-1)^n\rho_{nn}, \tag{3}$$

where the right-hand side can be construed as the expectation value of the photon number parity operator $\Pi=\sum_n(-1)^n|n\rangle\langle n|$. Since ρ_{nn} is the probability to count n photons in ρ, it is therefore clear that the value of the Wigner function at the origin can be obtained directly from the statistics of ideal PNR measurements. Banaszek and Wódkiewicz then proposed to access the Wigner function in the rest of the quantum phase space by simply displacing the quantum state ρ by $\alpha=(q+ip)/\sqrt{2}$. In practice, this can be achieved by combining the quantum signal with the coherent state $|\alpha\rangle$ of a well-stabilized laser beam, at a beam splitter of field transmission and reflection coefficients t and r, respectively ($r^2+t^2=1$). If the beam splitter transmits the quantum mode to be measured and reflects the coherent mode (for example), then the Wigner function measured by PNR statistics at the beam splitter's output will be [6]

$$W_{\mathrm{out}}(0,0)=\frac{1}{T}W\left(\frac{r}{t}q,\frac{r}{t}p;-\frac{r}{t}\right), \tag{4}$$

where the function $W(q,p;s)$ on the right-hand side is the s-ordered quasi-probability distribution [19], which coincides with the Wigner function for order parameter $s=0$. Hence, by choosing $r\simeq 0$ and by scanning $\alpha=(q+ip)/\sqrt{2}$ in the (q,p) phase space, we can measure the complete Wigner function of ρ.

Note that the single-TES restriction of the maximum number of measurable photons (here 5 photons at 1064 nm) entails a restriction of the Hilbert space to the Fock-state basis $\{|0\rangle,|1\rangle,|2\rangle,|3\rangle,|4\rangle,|5\rangle\}$. As noted in Ref. [11], when the average detected photon number approaches the cutoff limit of the detector, statistical errors increase drastically. Therefore, this quantum tomography method requires states with negligible probabilities of measuring photon numbers higher than five. However, this is not a sharp limitation: with eight independent TES channels our system could achieve, in principle, PNR detection up to 40 photons, and sophisticated data processing methods mentioned in the next section allow us to push that limit even farther away.

3. PNR DETECTION SETUP

Our TES system contains eight fiber-coupled thin-film tungsten devices fabricated at the National Institute of Standards and Technology, optimized for detection at 1064 nm [16]. The TES devices were cooled by a cryogen-free adiabatic demagnetization refrigerator and temperature stabilized at 100 mK. The TES detector is voltage biased [20], and self-heats into the superconducting transition illustrated in Fig. 1. When a photon is absorbed, the energy of the photon is thermalized in the electrons of the TES and there is a small temperature rise that causes a small measurable increase in the resistance of the TES. The change in resistance causes a change in current flowing through the device, which is measured using a SQUID amplifier system.

Two-photon absorption causes a larger temperature change and therefore a larger signal than single-photon absorption, and this results in photon-number resolution.

Since each quantum of light that is absorbed within the cooling time raises the temperature, and therefore the resistivity, of the device and since that resistivity change constitutes the exploitable TES signal, the maximum measurable photon number is ultimately determined by the amplitude of the steep transition slope (Fig. 1): upon reaching its top, the TES will saturate if additional photons are absorbed. There exist, however, methods to cope with such undesirable conditions as TES saturation: on the one hand, the cooling time would still provide information about the photon number in such an optical pulse if no more photons were impinging until cooling was complete [21]. Moreover, the saturation does not completely erase all photon-number information (unlike the schematic plot of Fig. 1, the resistance does retain a weaker dependence on temperature in the normal conducting regime) and a recent, more sophisticated analysis [22] can

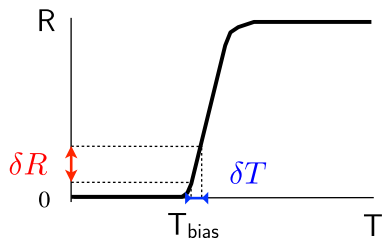

Fig. 1. Principle of operation of the TES. When the TES is temperature-biased at the edge of the superconducting transition T_{bias}—or on the steep transition slope—any temperature variation δT due to photon absorption is translated into a measurable resistance change δR.

also yield higher photon-number statistics into the saturation regime.

A. Signal Acquisition

The TES signal is composed of a rising edge of about 700 ns, corresponding to the response time of the TES detection chain, followed by a cooling decay tail of a couple μs. Figure 2 displays a typical example. Note that the detector is still active during the cooling tail and that there is no dead time as long as the TES is on the transition slope.

The TES signal was then sampled at a sampling rate of 5 Ms/s. The data was saved in packets of 2^{22} points. Each point was saved on the computer as a 16 bit integer, but only 14 bits were useful from the digitizer. Therefore, the size of each packet was 8 MBytes. This process could be repeated if necessary to join multiple data packets. Each data packet corresponded to 0.84 s of uninterrupted data. In this experiment, all Wigner function measurement data was exactly 1 packet long and contained no dead time.

B. Signal Processing and Photon "Pileups"

In all experiments, continuous-wave (CW) optical fields were measured and all TES signals were derived from continuous photon streams. Figure 3 displays an example of PNR detection with the TES, over a longer time range than Fig. 2. In the data of Fig. 3, the photon flux was kept low enough that all detection peaks were separated by more than the TES cooling time. In other words, there was no "photon pileup" event in which another photon impinged on the TES shortly after a first photon, while the signal is still on the decaying tail. An example of pileup is the rightmost (double) peak in Fig. 4(a). However, one can still observe small fluctuations in the detection peak heights in Fig. 3 due to noise in the readout electronics. In order to achieve accurate photon counting, including in the presence of pileups, we adopted the following procedure, whose steps are illustrated in Fig. 4.

First, we identified each detection event by finding rising edges in the signal. A rising edge is defined as a detection event if it rises to at least 40% of the average height of the single photon above the mean noise level. This threshold is set manually during the calibration process. For example, in Fig. 2, the threshold would typically be at 200 arb. units. The

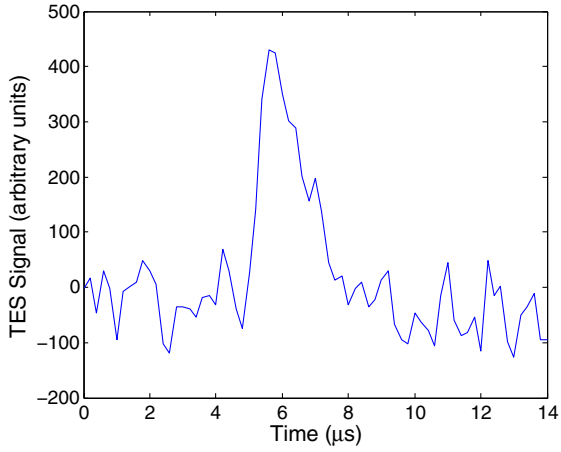

Fig. 2. Example of raw TES data showing a single photon detection event. The detection peak can be clearly distinguished from the noise.

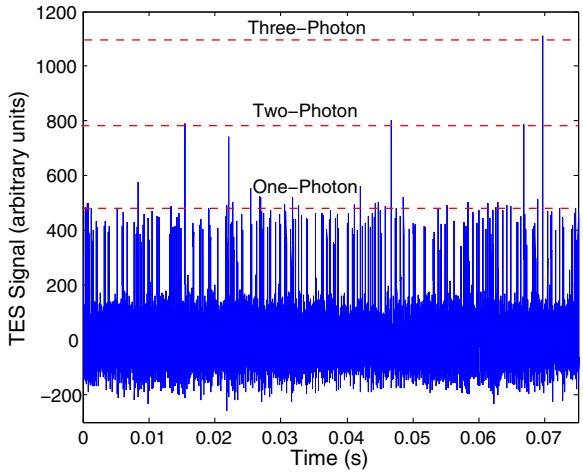

Fig. 3. Raw TES data for a CW beam showing distinct one-, two-, and three-photon peaks. The corresponding signal levels are indicated by the red dashed lines.

starting time of each detection event is recorded. Figure 4(b) displays the event times corresponding to the signal in Fig. 4(a). The algorithm then stores the maximum signal in the 1.2 μs following each starting time, and this maximum is stored as well [see Fig. 4(c)]. The TES response time is thus 1.2 μs. Hence, if two photons were absorbed within 1.2 μs of each other, they would be counted as one two-photon event and not as two one-photon events; this is determined in the final, quantization stage. First, we form the histogram of recorded signal heights, displayed in Fig. 5, where we can clearly see three well-separated peaks (the "zero-photon" area is likely due to blackbody radiation). From this histogram, we can now define the photon-number quantization thresholds. Using these thresholds, the quantized photon-number signals can be obtained and are displayed in Fig. 4(d). Note that the rightmost pileup peak is resolved here and accounted for as two one-photon events.

C. Detection Efficiency

The detector efficiency is an important factor in accurate state reconstruction. Losses not only change the state being measured but also introduce noise into the statistics. Detailed analysis of the effect of loss can be found in Refs. [6,11] and the references therein. Highly nonclassical states are very strongly affected and quickly lose their characteristics. For example, squeezed states become less squeezed under the action of losses. Coherent states, however, remain coherent states and only see their amplitude decrease. A detailed treatment [11] shows that losses only decrease the observed peak of the coherent state Wigner function, but preserve its Gaussian nature and width.

In this work, we restricted ourselves to coherent states. Our preliminary characterization of the overall system detection efficiency of our TES found it to be at least 70% and as high as 90%.

4. QUANTUM TOMOGRAPHY SETUP AND PROCEDURE

A. Setup

The experimental setup schematic is depicted in Fig. 6. The whole experiment was set up on a 24 in. thick floating optical

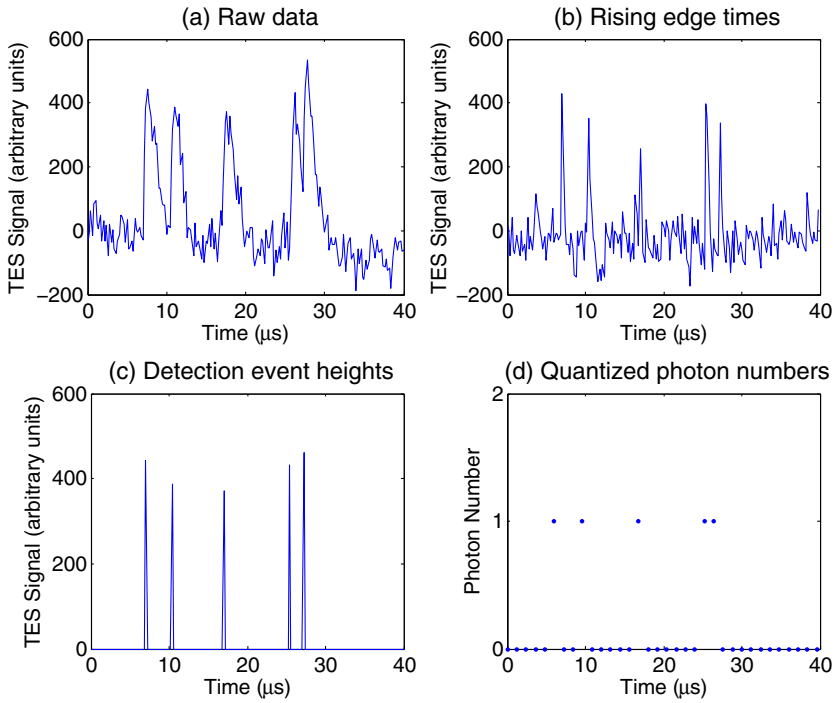

Fig. 4. Steps in the processing of raw analog data into quantized photon-count data. (a) A small sample of the raw data shows three single peaks and one "piled up" double peak, where the last photon was detected before the detector was cooled back to the nominal bias temperature. (b) Rising edge detection results. The procedure correctly detected five rising edges. (c) Encoded signals, made of the photon detection times along with the value of the maximum peak height within 1.2 μs of each event. (d) Final quantized photon counts determined using the thresholds defined in the histogram of peak heights in Fig. 5.

table and all optical paths were protected from air drafts by acrylic plastic enclosures. All light was emitted at 1064 nm by a monolithic Nd:YAG laser of high intrinsic stability (1 kHz FWHM linewidth). The optical mode was coupled to single-mode fibers, antireflection (AR) coated at 1064 nm by way of AR-coated aspheric lenses, and a 5-axis fiber aligner for 1550 nm light. These fibers entered the cryostat via throughputs and were then directly coupled to the superconducting detectors by silicon micromachined self-alignment [23]. As mentioned previously, measuring the Wigner function requires, besides PNR detection, quantum state displacement over the whole region of interest of the phase space. The displacement operator was implemented by interfering the signal

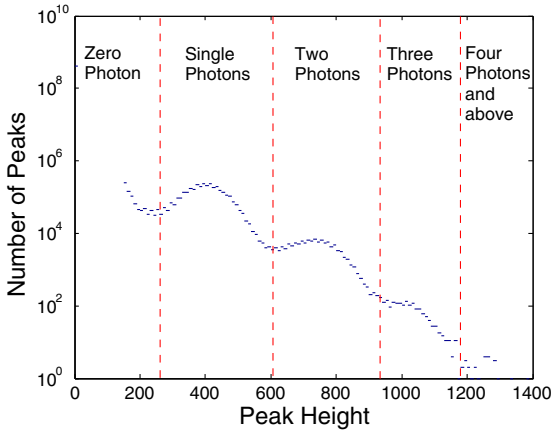

Fig. 5. Histogram of peak heights from the sample of Fig. 4(a). The histogram bins define the photon-number quantization thresholds.

field with a LO coherent field at a nearly fully transmitting beam splitter. The justification of this arrangement is easy to conceive when first considering the operator for a beam splitter of field reflection coefficient r, onto which two fields a and b are impinging,

$$e^{2i \arccos r(a^\dagger b + a b^\dagger)}. \tag{5}$$

If field a is in a coherent state $|\alpha\rangle$, the operator may be written as

$$e^{2i \arccos r(\alpha^* b + a b^\dagger)}, \tag{6}$$

which coincides with a displacement operator. The final step is to choose $r \simeq 1$ or $r \ll 1$ in order to ensure that the quantum signal b is not actually split in a significant way. The interference visibility of the signal and LO fields was $v = 98\%$. The amplitude $|\alpha|$ and phase $\arg(\alpha)$ of the transmitted coherent field were respectively varied using an amplitude electro-optic modulator (EOM) and a piezotransducer-actuated mirror. The EOM we used was a homemade device built out of an X-cut, 20-mm-long $RbTiOAsO_4$ (RTA) crystal, which was temperature controlled to about 1 mK by a commercial temperature controller. The voltages applied to EOM and piezo mirrors were generated by low-noise, high-voltage drivers controlled by the analog output ports of a lock-in amplifier. The lock-in amplifier was computer-controlled to output desired voltages through its auxiliary A/D outputs, which have 1 mV resolution, ±10 V range, and under 100 μs settling time. However, the fastest switching time we observed was 10 ms, which is likely a remaining limitation of the interface rather than the limit of the lock-in amplifier itself.

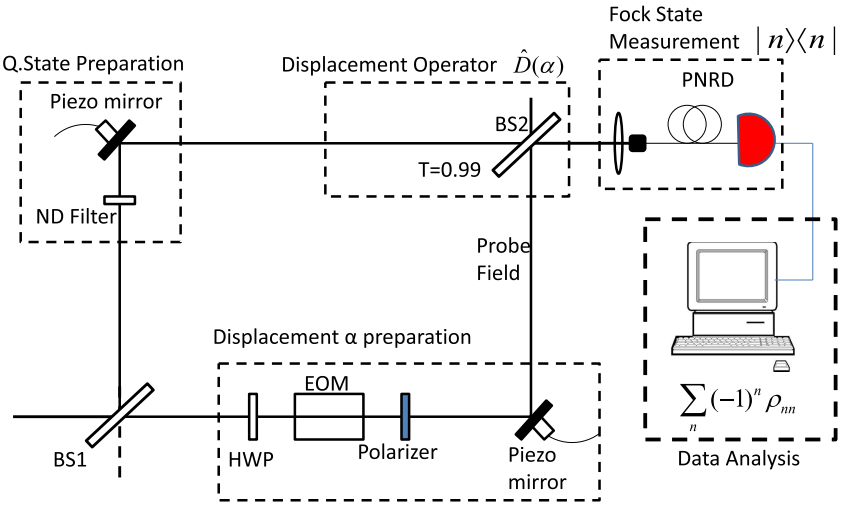

Fig. 6. Experimental setup for the quantum tomography of a coherent state using a coherent probe field and photon number measurements. The leftmost and upper optical path is that of the quantum state to be measured. The lower and rightmost optical path is that of the "local oscillator" whose field generates the phase-space displacement. BS, beam splitter; EOM, electro-optic modulator; HWP, halfwave plate; ND, neutral density.

B. Procedure

The amplitude $|\alpha|$ of the displacement field was varied in 40 steps while its phase $\arg(\alpha)$ went through 60 steps from 0 to 2π. At each point ($|\alpha|$, $\arg(\alpha)$) of the polar scan, the TES signals were processed to yield photon-counting statistics, hence photon-count probabilities and also parity measurements. Phase space scans consisted of sampling a sequence of circles with increasing radius, since changing the voltage applied to the EOM tuning $|\alpha|$ required a settling time of the order of 2 s, whereas $\arg(\alpha)$ could be scanned much faster as the phase modulator driver had much higher, 10 kHz, bandwidth. For each point in phase space, the TES output was digitized and processed to obtain the photon statistics in real time. The parity measurement was subsequently calculated from the statistics and saved.

5. RESULTS AND ANALYSIS

A. Reconstruction

In Fig. 7, we plot the measured Wigner functions of the vacuum, a weak coherent state, and a phase-diffused statistical mixture of coherent states. The phase diffusion was obtained by applying a 100 Hz sine waveform to the piezo mirror. The radial coordinate was obtained from the average number of photons detected for the blocked signal path. Thus, the graphs were parameterized with the complex variable $\beta = \sqrt{\eta}\alpha$, where α is the probe field reflected at the beamsplitter and η is the detection efficiency.

Each 0.84 s data packet (see previous discussion) was divided into bins of size $\tau = 0.1$ ms long, which amounted to about 8400 bins per point in phase space. The bin duration

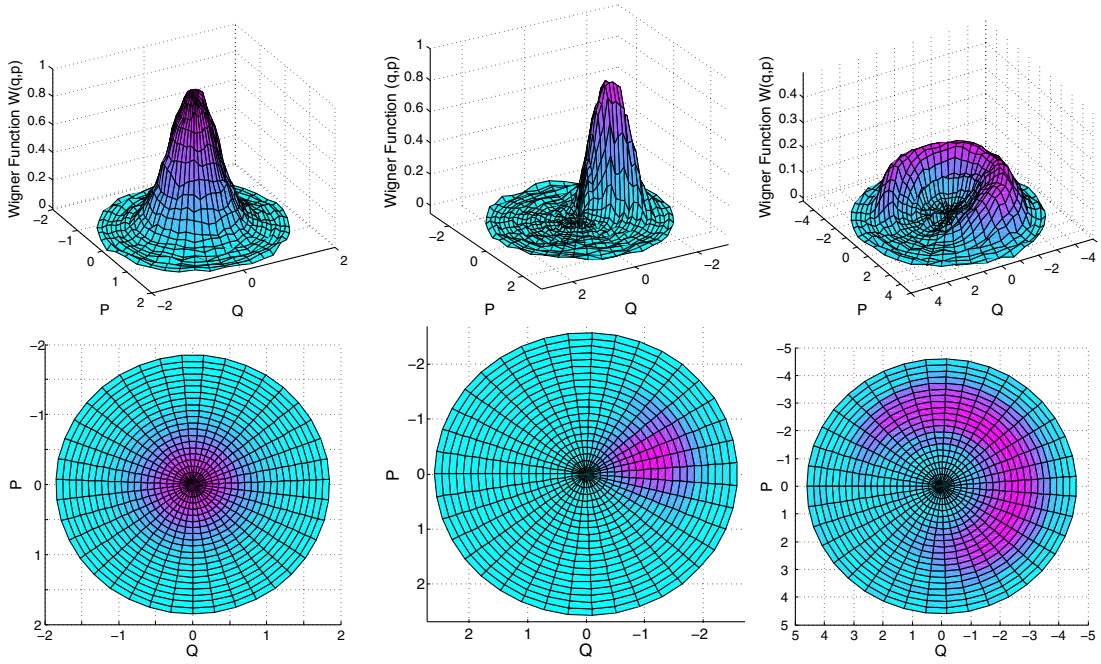

Fig. 7. Measured Wigner functions and contours of vacuum (left), coherent state (center), and phase-diffused coherent state (right). All plots are interpolated for 22 amplitude points and 40 phase points.

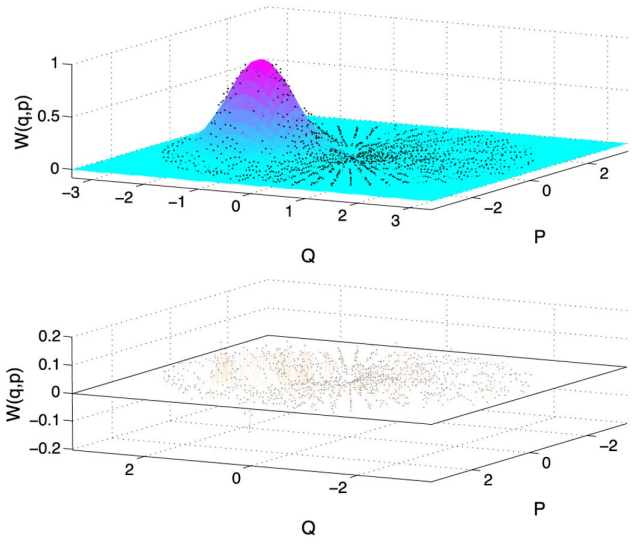

Fig. 8. Gaussian fit (top) and residuals (bottom) of the coherent-state tomographic data. The fit function was $W_{\text{fit}}(q,p) = a + b \exp[-m|(q-q_0)^2 + (p-p_0)^2|]$. The correlation coefficient was $R^2 = 0.966$.

defined the temporal envelope of the measured mode. Like in Banaszek's original experiment, this was shorter than the laser's coherence time (here, 1 ms) but of no consequence in the case of coherent states.

B. Verification

We investigated the weak coherent state case to verify the accuracy of our state reconstruction. The theoretical Wigner function of a coherent state $|\alpha_0\rangle$ is the well known

$$W(\alpha) = e^{-2|\alpha-\alpha_0|^2}. \tag{7}$$

However, a more realistic analysis [6,11] takes into account subunity detector efficiency, losses on the quantum signal, and the nonideal visibility of the signal–LO interference at the displacement beamsplitter BS2. The measured Wigner function is given by

$$W(\beta) = e^{-2\left|\beta-\sqrt{V\eta}t\alpha_0\right|^2-2(1-V)\eta t^2|\alpha_0|^2}, \tag{8}$$

where

$$V = \frac{v}{2-v} \tag{9}$$

is a measure of the overlap of signal and LO.

Table 1. Fit Results for Model Function[a]

Coefficients	Fit	Theory (10)
a	**0.000(2)**	**0**
b	**0.877(10)**	**0.867**
m	**1.72(3)**	**2**
p_0	0.248(6)	
q_0	1.532(6)	
$\sqrt{q_0^2+p_0^2}$	**1.552(6)**	**1.597**

[a] $W_{\text{fit}}(q,p) = a + b \exp[-m|(q-q_0)^2 + (p-p_0)^2|]$. Note that only the modulus $|\beta_0|$ was fitted, as its argument was arbitrary, if static, in the experiment. The values in boldface were the ones involved in the fit.

In this experiment, we had $v = 0.98$, $\eta = 0.72$, and $t^2 = 0.99$, yielding $V = 0.97$. We recall that the measured probe field in Fig. 7 is already β and the measured signal is $|\beta_0|^2 = \eta|\alpha_0|^2 = 2.553$; therefore, $|\beta_0| = 1.597$. Thus, our theoretical Wigner function was

$$W_{\text{fit}}(\beta) = 0.867e^{-2|\beta-1.597|^2}, \tag{10}$$

which we compared to a fit of the observed data in Fig. 7. The fit is plotted in Fig. 8 and the results are presented in Table 1. Note that the actual phase angle of the coherent state $[\arctan(p_0/q_0)]$ is not relevant here, even though we did fit it; only the amplitude $\beta_0 = \sqrt{q_0^2+p_0^2}$ is. Although the correlation coefficient of the fit was high ($R^2 = 0.966$), an inspection of Table 1 and of the residuals in Fig. 8 show that the agreement is only qualitative. We believe the reason for the discrepancy lies in systematic errors in the data acquisition, which lasted for 4000 s for the complete data. While our experimental setup is intrinsically very stable, there remain likely, if small, phase drifts over such a duration, since the optical phases are not locked. We plan to reduce the acquisition time and implement higher stability of the optical paths in the future.

6. CONCLUSION

In conclusion, we experimentally demonstrated quantum tomography with PNR measurements of more than one photon. We limited this initial investigation to the loss-immune coherent state and coherent-state mixture with phase noise and got reasonable agreement with expected values on key parameters. Since the detector's nonideal efficiency cannot be compensated in this method of measuring the Wigner function [6], it is only possible due to the recent development of high-efficiency PNR detectors. In future work, we will improve the performance of this method so as to make it applicable to accurate state reconstruction of highly nonclassical states, such as squeezed and Fock states, which first requires us to further increase the system detection efficiency. As suggested by Banaszek *et al.* [11], this method also generalizes very naturally to multimode tomographic reconstruction, which is a promising direction of research.

ACKNOWLEDGMENTS

This work was supported by the U.S. National Science Foundation, under grants PHY-0960047 and PHY-1206029, and by the University of Virginia.

REFERENCES

1. E. Wigner, "On the quantum correction for thermodynamic equilibrium," Phys. Rev. **40**, 749–759 (1932).
2. D. T. Smithey, M. Beck, M. G. Raymer, and A. Faridani, "Measurement of the Wigner distribution and the density matrix of a light mode using optical homodyne tomography: Application to squeezed states and the vacuum," Phys. Rev. Lett. **70**, 1244–1247 (1993).
3. U. Leonhardt, *Measuring the Quantum State of Light* (Cambridge University, 1997).
4. A. I. Lvovsky and M. G. Raymer, "Continuous-variable optical quantum-state tomography," Rev. Mod. Phys. **81**, 299–332 (2009).
5. R. Blume-Kohout, "Optimal, reliable estimation of quantum states," New J. Phys. **12**, 043034 (2010).

6. K. Banaszek and K. Wódkiewicz, "Direct probing of quantum phase space by photon counting," Phys. Rev. Lett. **76**, 4344–4347 (1996).
7. S. Wallentowitz and W. Vogel, "Unbalanced homodyning for quantum state measurements," Phys. Rev. A **53**, 4528–4533 (1996).
8. T. Kiss, U. Herzog, and U. Leonhardt, "Compensation of losses in photodetection and in quantum-state measurements," Phys. Rev. A **52**, 2433–2435 (1995).
9. M. Bondani, A. Allevi, and A. Andreoni, "Wigner function of pulsed fields by direct detection," Opt. Lett. **34**, 1444–1446 (2009).
10. M. Bondani, A. Allevi, and A. Andreoni, "Self-consistent phase determination for Wigner function reconstruction," J. Opt. Soc. Am. B **27**, 333–337 (2010).
11. K. Banaszek, C. Radzewicz, K. Wódkiewicz, and J. S. Krasiński, "Direct measurement of the Wigner function by photon counting," Phys. Rev. A **60**, 674–677 (1999).
12. K. Laiho, K. N. Cassemiro, D. Gross, and C. Silberhorn, "Probing the negative Wigner function of a pulsed single photon point by point," Phys. Rev. Lett. **105**, 253603 (2010).
13. S. Song, C. M. Caves, and B. Yurke, "Generation of superpositions of classically distinguishable quantum states from optical back-action evasion," Phys. Rev. A **41**, 5261–5264 (1990).
14. D. Achilles, C. Silberhorn, C. Śliwa, K. Banaszek, and I. A. Walmsley, "Fiber-assisted detection with photon number resolution," Opt. Lett. **28**, 2387–2389 (2003).
15. M. J. Fitch, B. C. Jacobs, T. B. Pittman, and J. D. Franson, "Photon-number resolution using time-multiplexed single-photon detectors," Phys. Rev. A **68**, 043814 (2003).
16. A. E. Lita, A. J. Miller, and S. W. Nam, "Counting near-infrared single-photons with 95% efficiency," Opt. Express **16**, 3032–3040 (2008).
17. G. Brida, L. Ciavarella, I. P. Degiovanni, M. Genovese, L. Lolli, M. G. Mingolla, F. Piacentini, M. Rajteri, E. Taralli, and M. G. A. Paris, "Quantum characterization of superconducting photon counters," New J. Phys. **14**, 085001 (2012).
18. S. M. Barnett and P. M. Radmore, *Methods in Theoretical Quantum Optics* (Clarendon, 1997).
19. K. E. Cahill and R. J. Glauber, "Density operators and quasiprobability distributions," Phys. Rev. **177**, 1882–1902 (1969).
20. K. D. Irwin, "An application of electrothermal feedback for high resolution cryogenic particle detection," Appl. Phys. Lett. **66**, 1998–2000 (1995).
21. E. Figueroa-Feliciano, B. Cabrera, A. J. Miller, S. F. Powell, T. Saab, and A. B. C. Walker, "Optimal filter analysis of energy-dependent pulse shapes and its application to TES detectors," Nucl. Instrum. Methods Phys. Res. A **444**, 453–456 (2000).
22. Z. H. Levine, T. Gerrits, A. L. Migdall, D. V. Samarov, B. Calkins, A. E. Lita, and S. W. Nam, "Algorithm for finding clusters with a known distribution and its application to photon-number resolution using a superconducting transition-edge sensor," J. Opt. Soc. Am. B **29**, 2066–2073 (2012).
23. A. J. Miller, A. E. Lita, B. Calkins, I. Vayshenker, S. M. Gruber, and S. W. Nam, "Compact cryogenic self-aligning fiber-to-detector coupling with losses below one percent," Opt. Express **19**, 9102–9110 (2011).